J Solid State Electrochem (2009) 13:1455–1465
DOI 10.1007/s10008-008-0722-0

ORIGINAL PAPER

Investigations of flow field designs in direct methanol fuel cell

Guo-Bin Jung · Cheng-Hsin Tu · Pei-Hung Chi · Ay Su · Fang-Bor Weng · Yur-Tsai Lin · Yu-Chun Chiang · Chi-Yuan Lee · Wei-Mon Yan

Received: 2 February 2008 / Revised: 5 October 2008 / Accepted: 23 October 2008 / Published online: 11 November 2008

Abstract An experimental and simulation research had been performed to investigate the performance as well as the flow distribution in the cathode flow field in the case of direct methanol fuel cells (DMFCs). The gas was well distributed in serpentine flow field, whereas stagnation of the gas was observed in parallel flow field. These would contribute to the cell performance greatly due to mass transfer effect when the cells start operating. In addition, the durability test of DMFC was drastically affected in parallel flow field due to poor ability to drain flooded water produced electrochemically at cathode and crossover from anode. In addition, pressure drops of different flow fields were also investigated to evaluate their contribution and feasibility as an economic application for DMFC. DMFC with serpentine flow field featuring higher pressure difference resulted in a larger parasitic energy demand. However, the optimal flow field designs are needed to balance the performance and pressure loss to achieve a uniform fluid distribution and simultaneously minimize energy demand for mass transport. Consequently, flow field with grid pattern appears to be the optimal design for the DMFC cathode.

Keywords Direct methanol fuel cell (DMFC) · Flow field · Stagnation zone · Pressure drop

G.-B. Jung (✉) · C.-H. Tu · A. Su · F.-B. Weng · Y.-T. Lin · Y.-C. Chiang · C.-Y. Lee
Department of Mechanical Engineering, Yuan Ze University,
135 Yuan-Tung Rd., Chung-Li,
Taoyuan 320 Taiwan, Republic of China
e-mail: guobin@saturn.yzu.edu.tw

G.-B. Jung · P.-H. Chi · A. Su · F.-B. Weng · C.-Y. Lee
Fuel Cell Center, Yuan Ze University,
135 Yuan-Tung Rd., Chung-Li,
Taoyuan 320 Taiwan, Republic of China

W.-M. Yan
Department of Mechatronic Engineering, Huafan University,
Shih-Ting,
Taipei 223 Taiwan, Republic of China

Introduction

Methanol is considered to be an attractive fuel because of its high energy density than hydrogen. It is an inexpensive liquid and can be handled, stored, and transported easily. In the consideration of safety, device fabrication, market, costs, and potential application issues, direct methanol fuel cells (DMFCs) appear to be the system of choice.

A thermodynamic reversible potential of a methanol oxygen fuel cell is 1.21 V at 25 °C [1]. In DMFCs, methanol is oxidized at the anode and oxygen is reduced at the cathode, while carbon dioxide (CO_2) and water are produced according to the following electrochemical half-reactions:

$$\text{Anode}: CH_3OH + H_2O \rightarrow CO_2 + 6H^+ + 6e^- \quad (1)$$

$$\text{Cathode}: 6H^+ + 6e^- + 3/2O_2 \rightarrow 3H_2O \quad (2)$$

The overall reaction can be represented as:

$$CH_3OH + 3/2O_2 \rightarrow 2H_2O + CO_2. \quad (3)$$

Thus, the overall cell reaction is found to be the electro-oxidation of methanol to CO_2 and water. All the reaction products both at anode and cathode sides should be effectively removed from the electrode structure and the cell in order to maintain an effective and continuous reaction. The competent removal of CO_2 at the anode is

one of the most important research issues in the development of DMFCs like the water removal at the cathode.

Many of the researchers investigated the anode flow characteristics, like volume flow variation [2], carbon dioxide monitoring [3], and flow bed characterization. Visually, investigations of the CO_2 gas evolution and flow behavior with flow beds based on stainless steel plate and mesh were also carried out [4–7]. The results showed promising behavior in terms of gas removal characteristics and electrical performance. Wong and Zhao [8] investigated the CO_2 bubble evolution effect on the performance of an in-house fabricated micro-DMFC. They found that the anode flow channel was blocked by elongated gas slugs periodically when the channel size was sufficiently small. They also noticed that the transient channel blocking phenomenon had significant impact on the cell performance.

In addition, water transport in the polymer electrolyte membrane of a fuel cell can occur via several modes, namely, by diffusion when there is a water activity gradient across the membrane, by electro-osmotic drag of proton migration when the cell is under operation, and by hydraulic permeation when there is a differential pressure across the membrane. As the water content in the polymer electrolyte membrane strongly affects membrane properties, reactant transport, and electrode reaction kinetics, it is essential to maintain an optimal water balance between the anode and cathode to achieve better cell performance [9]. The excess water accumulation in the cathode, from O_2 reduction and water transport across the membrane by electro-osmotic drag, will flood the cathode and, consequently, may block O_2 access to the catalyst sites. Uribe et al. [10] showed that the O_2 electrode kinetics at Pt/Nafion ionomer interface was reduced at a low water level.

Usually, under high current density operation conditions, electro-osmotic drag accounts for the majority of water transport across the membrane. It was observed that water transport in this mode from anode to cathode would dehydrate the anode and flood the cathode in H_2/O_2 polymer electrolyte fuel cells (PEFCs) [11, 12]. Ren and Gottesfeld [9] observed that dilute aqueous methanol solution fed to the anode had a significant advantage in DMFCs by maintaining high proton conductivity in the membrane in a wide range of current densities and temperatures. However, a penalty associated with liquid feed at the anode is the high flux of liquid across the membrane and into the DMFC cathode, which is an increase with cell current density. Such a liquid flux would bring about significant air cathode performance limitations, requiring high air flow at elevated pressure to secure higher cathode performance.

To ensure free access for reactants to the electrodes especially at high current density, products have to be removed from the cell. This can be achieved by diffusion layers and flow channels manufactured into plates. The main tasks of these flow field plates are to act as current collectors and distribute the fuel or air over the reaction surface area as well as remove the products from the cell. Presently, symmetrically grid flow fields (GFFs), serpentine flow fields (SFFs), and parallel flow fields (PFFs) are mainly used for both anode and cathode to facilitate mass transportation to and from the active area [12–15]. The serpentine flow field features high pressure drops between the inlet and the outlet and results in higher parasitic energy. Especially in the case of small portable fuel cell systems, the energy required to transport the fluids should be as small as possible. Flow fields with grid and parallel channels exhibit lower pressure differences, but inhomogeneous reactant gas distribution can easily occur. Like water and carbon dioxide, products of the electrochemical reactions can clog single channels as visualized and parts of the active area are bypassed [16, 17]. As previously reported in several publications, flow field design has a high influence on the performance stability of PEFCs and DMFCs [18–22].

Recently, Dohle et al. [23] studied the interaction between the diffusion layer and the flow field with a meander channel bipolar plate in a direct methanol fuel cell. Based on numerical simulations, they concluded that even a meander structure distribute the reactants non-homogeneously on the electrodes. Barreras et al. [24] investigated the flow distribution in a bipolar plate of a commercial PEFC experimentally and numerically. To this end, flow visualization using laser-induced fluorescence, as well as measurements of the velocity field by dye trace tracking, has been applied. On the other hand, a two-dimensional numerical simulation of the flow distribution based on the Navier–Stokes equations has also been performed.

In the present investigation, we report the effects of flow field designs on the performance of DMFC. Results obtained from both experimental and simulation studies have been compared and evaluated. Based on the results of previous study [25, 26], parallel flow field design was found to be optimal and used for anode in this investigation. Therefore, different flow field designs for cathode side were studied and simulated for their effects on flow pattern and performance.

Experimental

Membrane electrode assemblies (MEAs) with active area 25 cm^2 were purchased from Johnson Matthey. The MEAs composed of Nafion 115 membrane as electrolyte, and membrane was coated with catalyst. The gas diffusion layers are Toray TPGH-060 for both anode and cathode.

The catalyst loading is 3 mg Pt–1.5 mg Ru cm^{-2} on the anode side and 4 mg Pt cm^{-2} on the cathode side. The reactant for anode and cathode were pure oxygen and 2 M methanol solution with a flow rate of 150 ml cc^{-1} and 5 ml min^{-1}, respectively.

Flow fields were milled into the graphite material SIGRACET® BPP5 from SGL Technologies GmbH. Five different flow field designs including serpentine flow field type I (SFFI), serpentine flow field type II (SFFII), serpentine flow field type III (SFFIII), GFF, and PFF are presented in Fig. 1. All flow fields include a reaction area of 2,500 mm^2(50 mm long and 50 mm wide). Open areas were 1,396 mm^2 for PFF, 1,932 mm^2 for GFF, 1,344 mm^2 for SFFI, 1,924 mm^2 for SFFII, and 1,933 mm^2 for SFFIII.

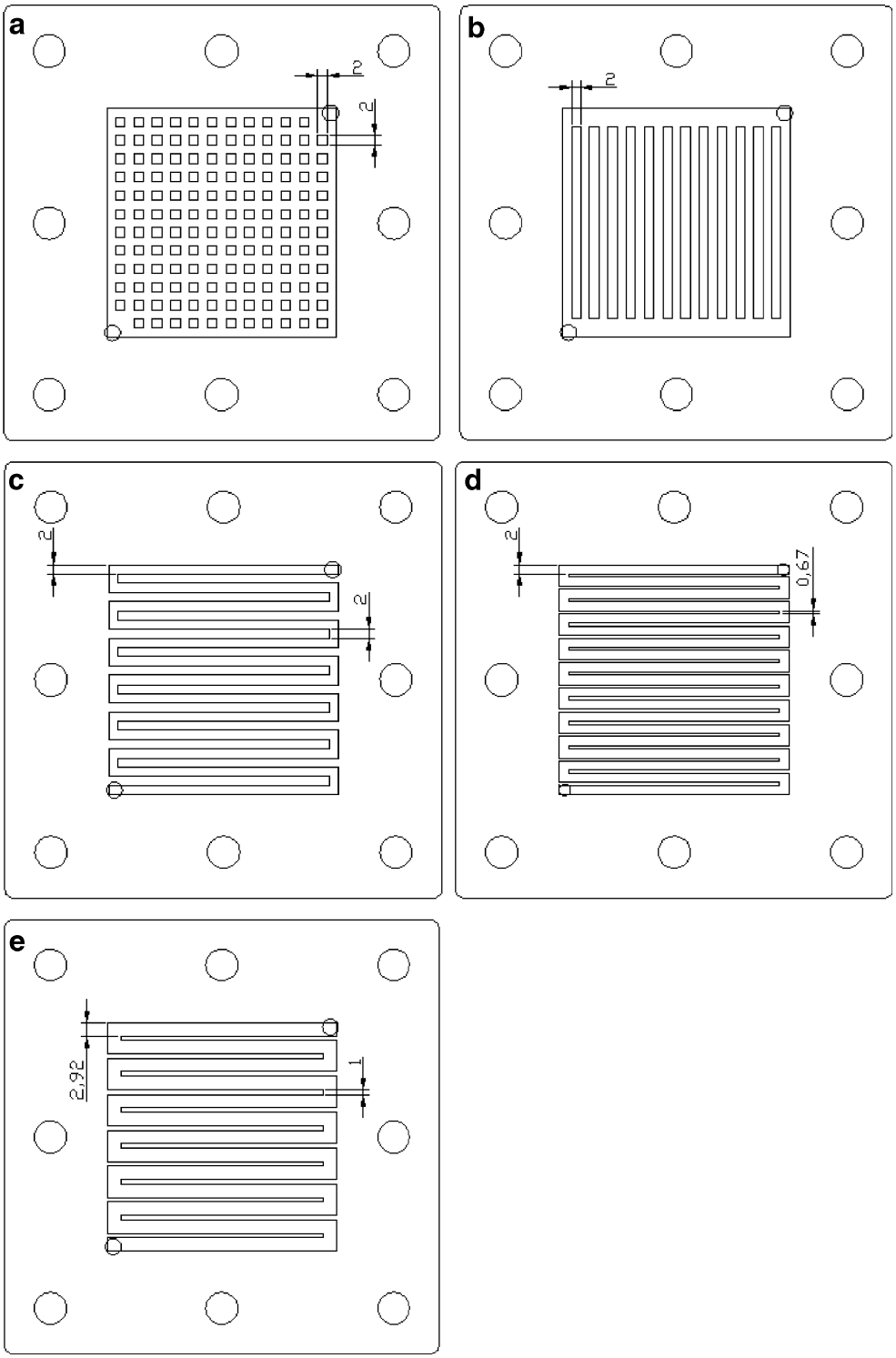

Fig. 1 Investigated flow fields for DMFC grid (**a**), parallel (**b**), serpentine I (**c**), serpentine II (**d**), and serpentine III (**e**)

SFFII, SFFIII, and GFF have similar open section areas. The flow field plates were 6.5 mm thick, 100.0 mm wide, and 100.0 mm long. All gas channels were 2.0 mm deep. To avoid corrosion, brass current collectors were coated with gold film. As can be seen from Fig. 2, the single cell in the present study includes one MEA, two flow field plates, two rubber gaskets, and two current collectors. In addition, a tape heater attached to the extension area is used to keep the operating temperature at 70 °C throughout the present study.

The test system is designed by ElectroChem, which consists of one instrument system (SA890B) and one CompuCell GTR system (FCT 2000). The instrument system (SA890B) is made by Scribners Associates. The Scribners Associates' SA890B series including electronic loads is computer-controlled. This control system consists of a bank of semiconductor devices conducting a large amount of current equal to or greater than the fuel cell output. Before the performance test, a nitrogen (N_2) tank is opened using the control system to purge the impurities within the flow piping and the cell. Reactant flow rates are 5 and 150 ml min^{-1} for the methanol solution and pure oxygen, respectively. Methanol is mixed with water, and the solution is pumped into the cell by a micropump (Micropump, Vancouver, WA, USA), while the O_2 flow rates are preset using the flow controller within the CompuCell GT® system made by MKS Instruments.

Half-cell simulation theory

A three-dimensional model has been developed to simulate cathode oxygen concentration of DMFCs by a half-cell model which is based on Gurau et al. [27] and Chu et al. [28]. The model accounts simultaneously for flow inlet, outlet, and oxygen consumption at catalyst surface boundary conditions. A single set of conservation equations of mass, momentum, and user scalar (oxygen mass concentration) are developed and numerically solved using a finite volume based with upwind scheme computational fluid dynamics technique (by CFDRC commercial code).

To simplify and save time setting up the simulation model, the user scalar mode of CFDRC is used to simulate the oxygen consumption at catalyst surface (very thin layer assumption) and diffusion layers. The user scalar transport equation is shown as [29]:

$$\frac{\partial \rho\phi}{\partial t} + \nabla \times \left(\rho \vec{V}\right)\phi = \nabla \times (D\nabla\phi) + S_\phi. \tag{3a}$$

The generic transport equation of a User Scalar ϕ follows the conservation form. The first term on the left hand side of Eq. 3a is the time rate change of the scalar (oxygen mass concentration per unit volume). The second term on the left-hand side and the first term on the right-hand side were used to describe the net mass flow across the control volume's boundaries and are named convection and diffusion terms, respectively. The second term on the right-hand side is used to describe the volumetric source or sinks term.

Half-cell catalyst layer equation

In the catalyst layer, oxygen is consumed and the transportation equation becomes:

$$\frac{d}{dx}\left(\varepsilon_c^{\tau_c}\rho D_{O_2}\frac{dY_c}{dx}\right) = \frac{j}{4F}M_{O_2}. \tag{3b}$$

With the assumption of irreversible oxygen reduction reaction, first order of oxygen activity, and electroneutrality holds for any representative elementary volume, the cathode transfer current density could be expressed as:

$$j = 2F\kappa Y_c e^{\left(\frac{2\alpha F\eta}{RT}\right)}. \tag{3c}$$

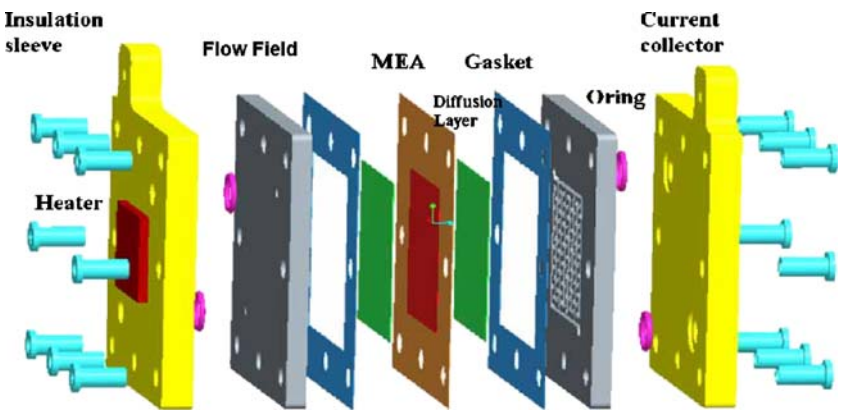

Fig. 2 Schematic illustration of homemade single cell

Table 1 Number of computational domains on each region of different types of flow field

Type of flow field	Cathode channel (2 mm)	Cathode diffusion + catalyst layer (0.2 mm)	Total number of cells	Total number of nodes
Serpentine (SFF)	86,272	160,000	246,272	299,097
Parallel (PFF)	95,488	160,000	255,488	307,497
Grid (GFF)	123,648	160,000	283,648	335,777

The density is computed according to the ideal gas law:

$$\rho = \frac{PM}{RT} \tag{3d}$$

The model in this study includes flow fields and gas diffusion layers. Based on Eqs. 3c and 3d, Eq. 3b becomes:

$$\varepsilon_c^{\tau_c} \rho D_{O_2} \frac{dY_c}{dx} \approx \frac{1}{2} M_{O_2} \kappa \Delta x e^{\left(\frac{2\alpha F\eta}{RT}\right)} Y_c \tag{3e}$$

where ε_c is the effective porosity of catalyst, τ_c is tortuosity of catalyst, ρ is density of oxygen, M_{O2} is molecular weight of oxygen, κ is reaction rate constant, η is surface overpotential of catalyst, F is Faraday constant, Δx is thickness of catalyst layer, and Y_c is the gas concentration of inlet.

Equation 3e is rearranged and becomes:

$$D_{O_2} \frac{dY_c}{dx} = \frac{M_{O_2} \kappa \Delta x}{2\varepsilon_c^{\tau_c}} e^{\left(\frac{2\alpha F\eta}{RT}\right)} Y_c. \tag{3f}$$

Half-cell catalyst boundary condition

Based on CFDRC, the general boundary condition can be expressed as:

$$aD_{O_2} \frac{dY_c}{dx} + bY_c = c. \tag{3g}$$

Equation 3g would reduce to type 1 (Dirichlet) or type 2 (Neuman) boundary condition when a or b equals to 0.

The diffusion layer boundary condition for cathode oxygen gas concentration must be equal to the consumption of oxygen in catalyst layer because the models include the diffusion layers and flow fields only. Equation 3g needs further arrangement to fit with the form of Eq. 3f, that is $a=1$, $c=1$, and Eq. 3g becomes:

$$D_{O_2} \frac{dY_c}{dx} = bY_c. \tag{3h}$$

Equations 3e and 3h are compared and result in:

$$b \approx \frac{M_{O_2} \kappa \Delta x}{2\varepsilon_c^{\tau_c}} e^{\left(\frac{2\alpha F\eta}{RT}\right)}. \tag{3i}$$

Based on Eq. 3i, η is substituted to get the value b, and oxygen consumption of the whole cell reaction can be simulated by transforming the boundary condition of diffusion layer to oxygen consumption.

Half-cell computational domains

A three-dimensional model of transport phenomena within the DMFC cathode side includes gas channel, gas diffusion layer, and thin catalyst layer (only a plane). There are 200 elements in the x-direction, 200 elements in the y-direction, and four elements in the z-direction, for a total of about 160,000 elements or cells for gas diffusion and catalyst layers. Serpentine, parallel, and grid flow channels are constructed and simulated. Serpentine flow channel includes 21,568 cells, while there are 23,872 cells and 30,912 cells for the parallel flow channel and the grid flow channel in the x–y planes, respectively. All flow channels include four cells in the z-direction. Dimensions of the computational domains are summarized in Table 1.

Adopted for the convergence criterion and the minimum residual value are 1.0×10^{-6} and 1.0×10^{-18}, respectively. The inlet of oxygen mass concentration (2.9025×10^{-6}) is fixed for different flow patterns. There are two ways for oxygen output from the system, one is outlet and the other is electro-chemical reaction on catalyst plane. The oxygen concentration on each region for different flow patterns and its total imbalance are summarized in Table 2. The total imbalance is all below six orders less than inlet oxygen mass concentration; therefore, the numerical results are fully converged.

Table 2 Oxygen mass concentration at different surfaces and total imbalance

Type of flow field	Channel inlet	Channel outlet	Catalyst consumption	Total imbalance
Serpentine (SFF)	2.9025E−6	−3.1851E−7	−2.5840E−6	5.3999E−14
Parallel (PFF)	2.9025E−6	−3.4438E−7	−2.5581E−6	2.4472E−12
Grid (GFF)	2.9025E−6	−2.1452E−7	−2.6880E−6	1.7109E−12

Results and discussion

The geometry of flow field channel impacts the fuel cell performance by affecting the flow and water management characteristics in the flow field. To design the channel geometry properly, one must understand how it affects performance, interacts with the MEA, and the limitation of formability of the materials involved.

In this study, commercial MEAs (Johnson Matthey) with five different flow field designs are used and step current discharge is performed with different stoichiometric factors. Proper pressure drops result in good mass transfer and exclude generated water effectively. However, higher pressure difference also leads to larger parasitic energy demand. Especially in the case of small portable fuel cell systems, the energy required to transport the fluids should be as small as possible. Thus, optimal DMFC design with net power output pressure drops are measured and compromised for different flow fields.

Pressure drop of different flow field designs

Flow in fuel cell is pressure-driven. Increasing pressure drop removes excess liquid water from the fuel cell easily [30], which improves the performance as water flooding to the catalyst layer was overcome. These performance gains must be balanced; otherwise, it would result in higher parasitic load of the system.

Effects of air flow on the pressure drops between the gas inlet and outlet of different flow field designs are presented in Fig. 3. The pressure drops increase with increasing air volumetric flow, whereas flow conditions resulted in a superposition of smooth (volume flow and pressure drop are linearly dependent) and non-smooth (volume flow and pressure drop are quadratic-dependent) regimes. The pressure drops of the serpentine designs are much greater than that of the parallel and grid ones. In addition, SFFII presented the biggest pressure difference, while SFF III presented the smallest.

Effects of cathode flow field designs on DMFC

The following experiments were undertaken to compare the performance of DMFCs with different cathode flow field designs. The current–voltage characteristics of DMFCs with serpentines, parallel, or grid flow fields were measured with a stoichiometric factor of 2.5. As can be seen in Fig. 4, the best DMFC performance can be obtained with the serpentine II flow field. By virtue of the pressure-driven mass flow in the channels, the mass transportation and removal of this water is easy by serpentine structures. In addition, the removal of generated water results in the replacement of fresh air which leads to a higher performance, depressing the sluggish mass transfer limitations.

The parallel flow field shows the worst performance due to the free accesses and bad distribution of reactant. In the parallel design, air and water at the cathode can frequently flow through some specific channels. In other words, specific channels are always occupied by reactants, while others remain unoccupied. Therefore, part of the cathode catalyst remains idle to convert fuel to power.

In the grid design, due to the vertical inlet of flow and the flow field characteristic, the flow pattern of the reactant becomes non-smooth, which leads to more uniform distribution than that of parallel design. Therefore, the grid structure presents good gas distribution and acceptable performance output even with the minimal pressure drops.

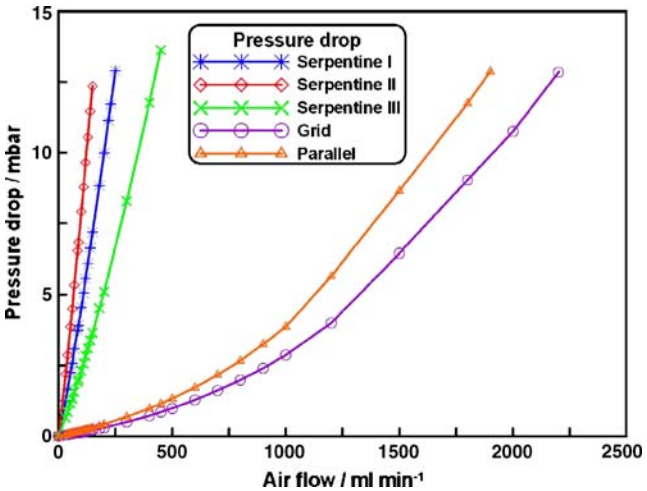

Fig. 3 Effects of flow rate on pressure drops on different air flow field designs

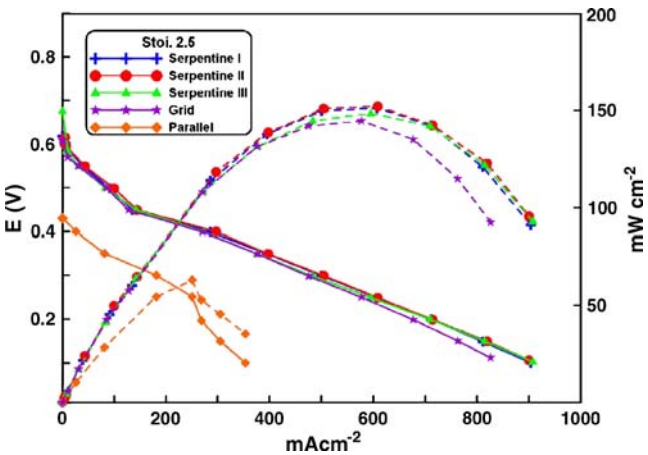

Fig. 4 I-E characteristics of DMFCs with different flow fields (Stoi. 2.5)

Effects of stoichiometric factor and methanol crossover on DMFC performance

In DMFCs, the flooding water is produced electrochemically at cathode and crossover from anode. The long-term behavior of the output voltage of the flow field designs are investigated for 3 h with stepwise constant current discharge using different stoichiometric factor as shown in Figs. 5 and 6. The cells are operated for 1 h at 6 A initially, corresponding to 240 mA cm^{-2}. Subsequently, the cell currents are increased to 10 A (400 mA cm^{-2}) and 16 A (640 mA cm^{-2}) and operated for 1 h.

The parallel flow field design resulted in water droplet coalescing in the channels and poor reactant gas distribution over the cathode catalyst. For the stoichiometric factor of 1.5, the performance of parallel design was unable to export. When running the cell for extended periods of time at 6 A with stoichiometric factor of 2.5, it was found that low and unstable voltages resulted. As the current increased to 10 A further, the voltage cannot be maintained and is interrupted intermittently as shown in Fig 5. In the parallel design, air and water in the cathode can frequently flow through specific channels. This will be further verified in "Flow field half-cell simulation on cathode". For grid flow field design, good distribution of reactant was caused by the non-smooth flow resulting from the vertical inlet gas and the block structure. Therefore, the grid structure showed more uniform distribution with high stoichiometric factor (e.g., 2.5) than that of parallel design even with minimal pressure drops.

The performances differ largely in terms of different stoichiometric factor, as shown in Figs. 5 and 6. It was clear from Fig. 6 which voltage was found to decrease with increase of operating current for the stoichiometric factor of 2.5. As the stoichiometric factor was lowered to 1.5, the voltage is lower for 6 A than that for 10 and 16 A, while the cell with grid flow field performed worse than that of serpentines. Operating the DMFCs with grid flow field with low flow rate resulted in less remarkable non-smooth effect and worse distribution of reactant thereafter. DMFC equipped with grid flow field with optimal flow rate was capable of performing similar to that with serpentine flow field, however, with lower parasitic energy demand.

On the case of the serpentine flow field designs, better mass transfer resulted in elimination of water effectively due to higher pressure drop. Thus, the cathode with serpentine flow field performed well and exhibited better stable performance. In addition, variation of serpentine flow field dimensions (serpentine I, II, and III) resulted in

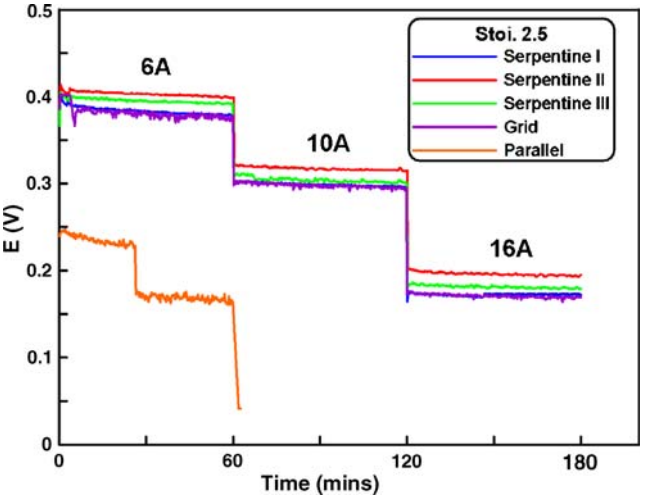

Fig. 6 Stepwise constant current discharge of different cathode flow field designs with stoichiometric factor of 2.5

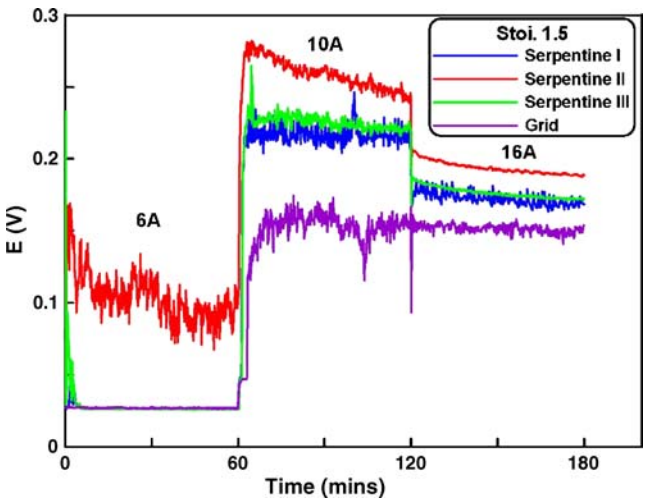

Fig. 5 Stepwise constant current discharge of different cathode flow field designs with stoichiometric factor of 1.5

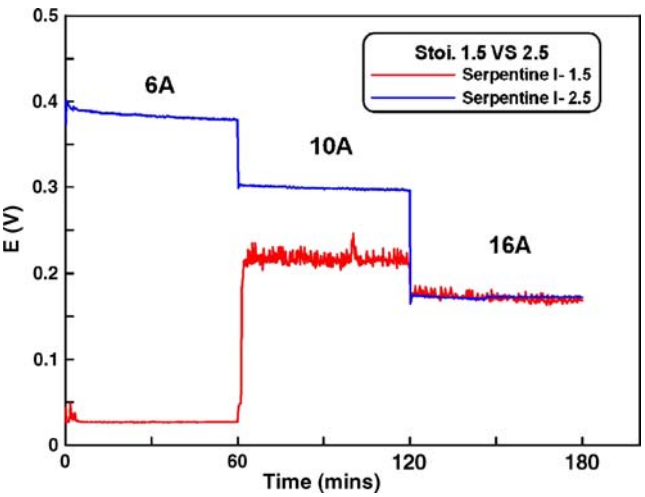

Fig. 7 Stepwise constant current discharge of serpentine I flow field design with different stoichiometric factors

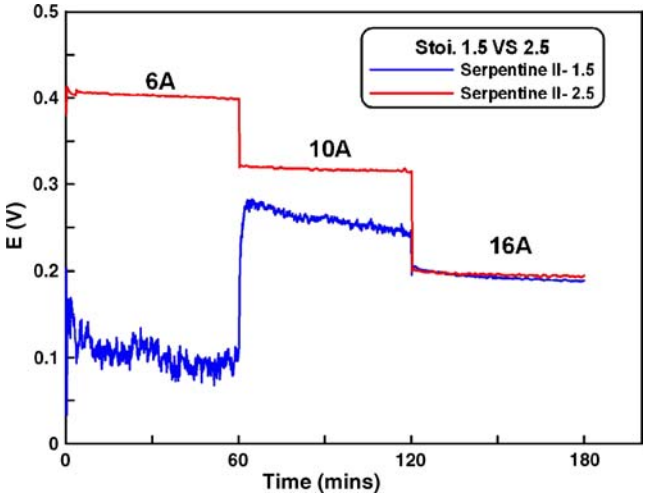

Fig. 8 Stepwise constant current discharge of serpentine II flow field design with different stoichiometric factors

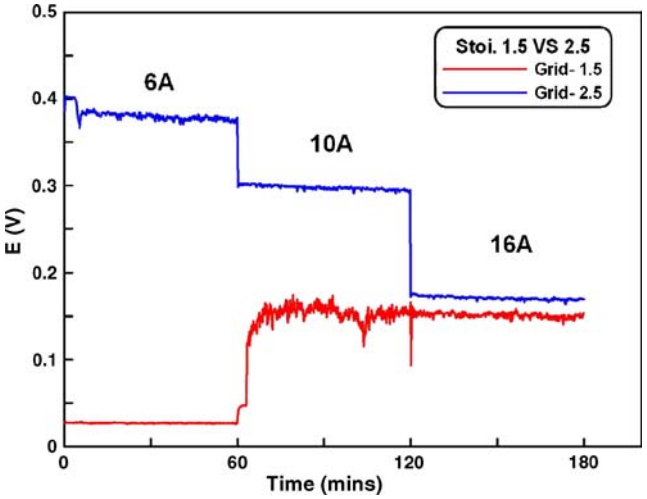

Fig. 10 Stepwise constant current discharge of grid flow field design with different stoichiometric factors

difference of pressure drop and reaction area (open section). As shown in Figs. 5 and 6, the order of the performance of the flow designs were found to be serpentine II, serpentine III, and serpentine I, respectively. Although the serpentine I structure possesses good mass transfer and could exclude water efficiently than serpentine III due to higher pressure drop, serpentine III (1,933 mm^2) with larger open section than serpentine I (1,344 mm^2) exhibited better performance. Furthermore, serpentine II, serpentine III, and grid structures hold similar open sections; performance difference depended on the pressure differential. Serpentine II performed better than that of grid and serpentine III due to higher pressure differential, as shown in Fig. 3.

Voltage exported of different flow field structures with the stoichiometric factor of 1.5 were shown in Fig. 5. Among these, serpentine II showed better performance at discharge of 6 A because of better mass transfer of oxygen led by large pressure differential as shown in Fig. 2. The voltage was found to vary with the stoichiometric factor of 1.5 (31.5 ml min^{-1}) than the stoichiometric factor of 2.5 (52.5 ml min^{-1}) at discharge of 6 A, as shown in Figs. 7, 8, 9, and 10. However, the voltage outputs were similar, while the cells operated at high current with different stoichiometric factor for different serpentine structures (serpentine I, II, and III). It was clear from Figs. 7, 8, 9, and 10 that the performance at discharge of 16 A did not enhance obviously when the stoichiometric factor was increased from 1.5 to 2.5. However, the flow rate was found to affect the non-smooth degree of the grid structure and resulted in slight voltage increase at higher current discharge as the

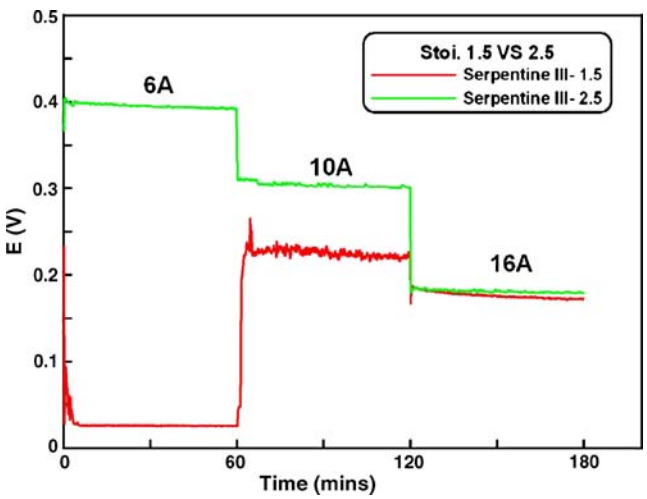

Fig. 9 Stepwise constant current discharge of serpentine III flow field design with different stoichiometric factors

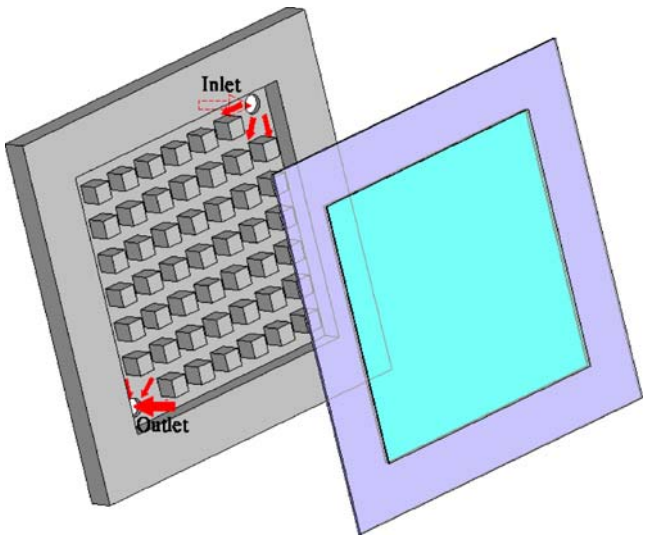

Fig. 11 Simulation model domain and flow direction

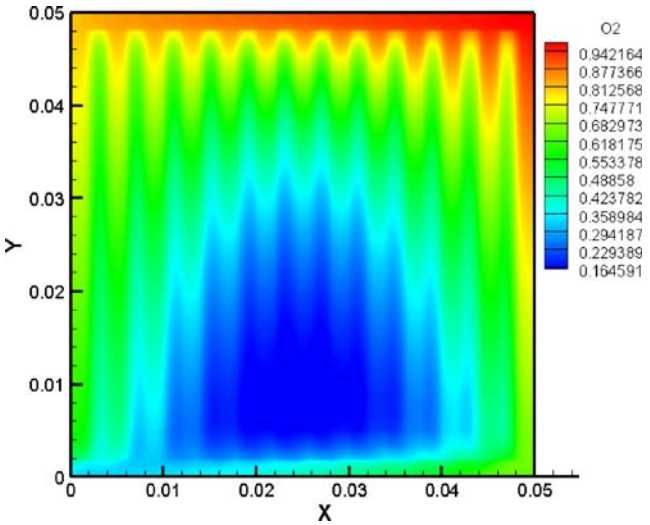

Fig. 12 Oxygen mass fraction with parallel flow field at high current operation (84 ml min^{-1})

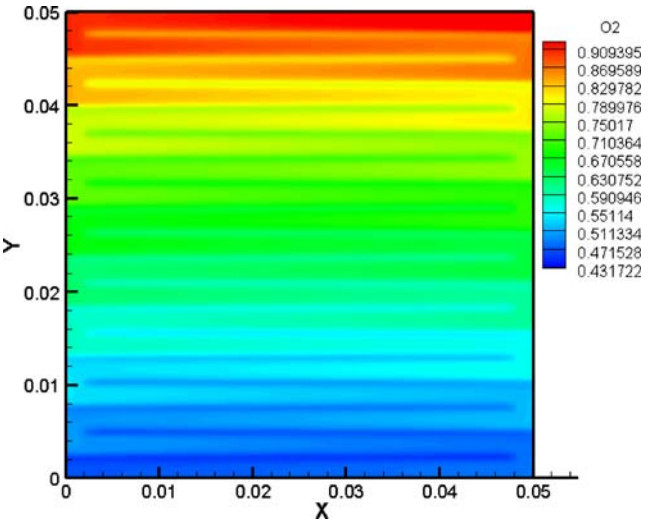

Fig. 14 Oxygen mass fraction with serpentine II flow field at high current operation (140 ml min^{-1})

stoichiometric factor was increased from 1.5 to 2.5, as shown in Fig. 10.

Methanol crossover through the electrolyte membrane may cause the overpotential and reduce the DMFC's performance. Higher methanol crossover will affect the utilization of fuel at anode as well as the overall performance of the DMFC. Higher oxygen contents are needed to react with methanol. Therefore, optimal oxygen flow not only provides enough content for reaction (both chemical and electrochemically) but also better water exclusion especially for grid design with less pressure differential. Methanol is utilized effectively and results in less methanol crossover at higher current discharge. Therefore, oxygen flow rate will not affect largely the cell performance.

Flow field half-cell simulation on cathode

The reactant gas flow distribution was simulated using half-cell reaction simulation models to determine the characteristics of different flow fields. Figure 11 shows the domain and flow direction of the simulation. Oxygen enters vertically to the flow field along the *Z*-axis and turns to *XY*-axes parallel to the gas diffusion layer. By using variable oxygen consumption, different operating currents can be simulated in this study.

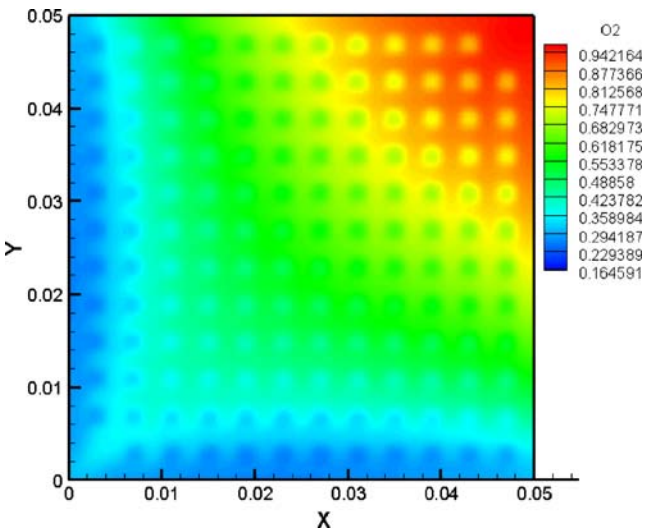

Fig. 13 Oxygen mass fraction with grid flow field at high current operation (84 ml min^{-1})

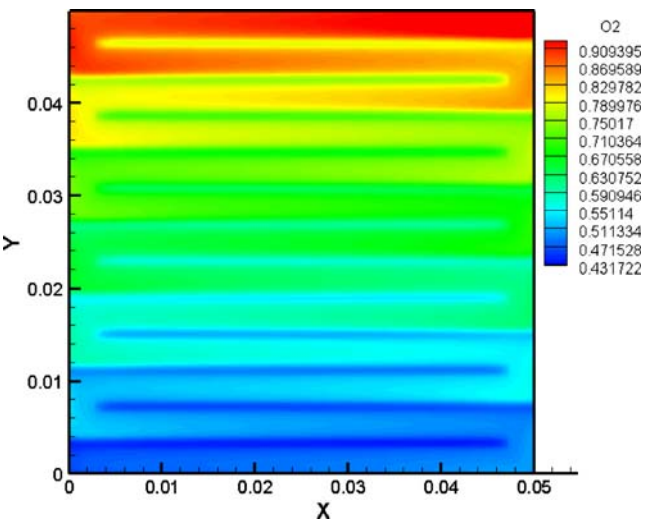

Fig. 15 Oxygen mass fraction with serpentine III flow field at high current operation (140 ml min^{-1})

Among the grid and parallel structures, the grid shows good distribution of reactant than parallel structure even with minimal pressure differential. As can be seen in Figs. 12 and 13, oxygen and water may flow in one or more of the many channels in the parallel and grid designs. For parallel flow field, however, bad distribution due to free roaming areas of gases causes barrenness. The barren region results in flooding water (produced electrochemically at cathode and crossover from anode) and bad mass transfer of reactants. Therefore, at high current operation, less reactant is provided for reaction and water removal. For the grid structure, good distribution of reactants caused by non-smooth flow results from vertical inlet gas and block structure. This is the reason why grid designs provide better gas distribution than that of the parallel design and improvement of the performance, as shown in Figs. 5 and 6.

For similar open section (reaction area) of flow fields, grid structure, serpentine II, and serpentine III, simulation results from Figs. 13, 14, and 15 show the distributions of oxygen. Although the grid design has good distribution resulted from block structure and vertical inlet, all oxygen and generated water have to flow through one and the only channel in serpentine structures and hold better mass transfer and can exclude water effectively. Therefore, cathode with serpentine flow field performs greatest and has most stable durability. For serpentine II and serpentine III, the simulation results show similar distribution pattern of oxygen. The performance differences led by the width of flow channel cause different flow velocity and result in different pressure drops, that is, the flow channel (serpentine II) with the narrow width holds higher flow velocity that provides good drainage. Thus, serpentine II shows better performance than serpentine III. The performances of similar open section were increased by the increasing pressure differentials, as shown in Figs. 3 and 6.

Conclusions

Effects of cathode flow field design on the performances of DMFCs were investigated. It was shown that various structures had a large impact on the stability of DMFC operation due to their different abilities to remove product water and CO_2, respectively. For low stoichiometric factor operation, serpentine flow fields exhibited both the highest and the most stable performance due to higher pressure drop for mass transfer and water removal ability. Grid and parallel designs suffered from water blocking in channels and exhibited worse performance. Thereby, inhomogeneous flow distribution occurs and parts of the cathode catalyst were bypassed. For medium stoichiometric factor operation, however, grid flow fields exhibited similar performance compared to that of serpentine I. The flow of the reactant became non-smooth in channels, which led to a more uniform distribution due to the vertical inlet of flow and the flow field characteristic for grid flow field. Therefore, the grid structure exhibited better performance and gas distribution even though minimal pressure drops. Consequently, flow field with grid pattern appeared to be the DMFC cathode design especially in the case of small portable fuel cell systems in which the energy required to transport the fluids should be as small as possible.

Nomenclature

M_{O2}	molecular weight of oxygen
κ	reaction rate constant (kmol m^{-3} s^{-1})
F	Faraday constant (96,487,000 C $kmol^{-1}$)
Y_c	gas concentration of inlet
Δx	thickness of diffusion layer (0.2 mm)
D_{O2}	diffusion coefficient (8.39×10^{-6} m^2 s^{-1})

Greek letters

α	transfer coefficient
ρ	density of oxygen (1.43 kg m^{-3})
ε_d	diffusion layer effective porosity (0.4)
τ_c	catalyst tortuosity (1.5)
η	surface overpotential of catalyst layer

Acknowledgment The authors would like to thank for the financial support by Bureau of Energy, Ministry of Economy Affair of ROC through grants 96-D0137-4.

References

1. Kordesch K, Simader G (1996) Fuel cells and their applications. VCH Publishing, Weinheim
2. Scott K, Taama WM, Kramer S, Argyropoulos P, Sundmacher K (1999) Electrochim Acta 45:945. doi:10.1016/S0013-4686(99)00285-6
3. Argyropoulos P, Scott K, Taama WM (1999) Electrochim Acta 44:3575. doi:10.1016/S0013-4686(99)00102-4
4. Yang H, Zhao TS (2005) Electrochim Acta 50:3243. doi:10.1016/j.electacta.2004.11.060
5. Yang H, Zhao TS, Ye Q (2004) J Power Sources 139(1–2):79. doi:10.1016/j.jpowsour.2004.05.033
6. Scott K, Taama WM, Argyropoulos P (2001) J Power Sources 79:43. doi:10.1016/S0378-7753(98)00198-0
7. Scott K, Argyropoulos P, Yiannopoulos P, Taama WM (2001) J Appl Electrochem 31:823. doi:10.1023/A:1017559124395
8. Wong CW, Zhao TS (2005) J Electrochem Soc 152(8):A1600. doi:10.1149/1.1949067
9. Ren X, Gottesfeld S (2001) J Electrochem Soc 148(1):A87. doi:10.1149/1.1344521
10. Uribe FA, Springer TE, Gottesfeld S (1992) J Electrochem Soc 139:765. doi:10.1149/1.2069299
11. Wilson MS, Springer TE, Davey JR, Gottesfeld S (1995) The Electrochemical Society Proceedings Series, Pennington, NJ, p 115

12. Nguyen TV (1996) J Electrochem Soc 143:L103. doi:10.1149/1.1836666
13. Wood DL, Yi JS, Nguyen TV (1998) Electrochim Acta 43:3795. doi:10.1016/S0013-4686(98)00139-X
14. Liu L, Pu C, Viswanathan R, Fan Q, Liu R, Smotkin ES (1998) Electrochim Acta 43:3657. doi:10.1016/S0013-4686(98)00123-6
15. Yi JS, Nguyen TV (1999) J Electrochem Soc 146:38. doi:10.1149/1.1391561
16. Tüber K, Pócza D, Hebling C (2003) J Power Sources 124:403. doi:10.1016/S0378-7753(03)00797-3
17. Argyropoulos P, Scott K, Taama WM (1999) Electrochim Acta 44:3575. doi:10.1016/S0013-4686(99)00102-4
18. Oedegaard A, Hufschmidt S, Wilmshoefer R, Hebling C, (2003) Second European Polymer Electrolyte Fuel Cell Forum, Publisher European Fuel Cell Forum, Oberrohrdorf, Lucerne, Switzerland, June 30–July 4
19. Bewer T, Dohle H, Beckmann T, Mergel J, Stolten D, (2001) Preceedings of the First European Polymer Electrolyte Fuel Cell Forum, European Fuel Cell Forum, Oberrohrdorf, Lucerne, Switzerland, July 2–6
20. Aricò AS, Cretì P, Baglio V, Modica E, Antonucci V (2000) J Power Sources 91:202. doi:10.1016/S0378-7753(00) 00471-7
21. Tüber K, Zobel M, Schmidt H, Hebling C (2003) J Power Sources 122:1. doi:10.1016/S0378-7753(03)00428-2
22. Wilkinson DP, Vanderleeden O (2003) Handbook of fuel cells, vol 3. Wiley, Chichester, UK, p 315
23. Dohle H, Jung R, Kimiaje N, Mergel J, Muller M (2003) J Power Sources 124(2):371. doi:10.1016/S0378-7753(03)00800-0
24. Barreras F, Lozano A, Valino L, Marin C, Pascau A (2005) J Power Sources 144:54. doi:10.1016/j.jpowsour.2004.11.066
25. Jung GB, Su A, Tu CH, Weng FB, Chan SH (2007) J Fuel Cell Sci Technol 43:65
26. Jung GB, Su A, Tu CH, Weng FB, Chan SH (2007) J Power Sources 171:212. doi:10.1016/j.jpowsour.2006.12.063
27. Gurau V, Barbir F, Lin H (2000) J Electrochem Soc 147:2468. doi:10.1149/1.1393555
28. Chu HS, Yeg C, Chen F (2003) J Power Sources 123:1. doi:10.1016/S0378-7753(02)00605-5
29. CFD-ACE (2003) Modules manual “user scalar modulus”
30. Xianguo Li, Sabir I, Park J (2007) J of Power Sources 163:933. doi:10.1016/j.jpowsour.2006.10.015